

Splitting of the Raman $2D$ band of graphene subjected to strain

M. Mohr,^{1,*} J. Maultzsch,¹ and C. Thomsen¹

¹*Institut für Festkörperphysik, Technische Universität Berlin, Hardenbergstr. 36, 10623 Berlin, Germany*

The Raman $2D$ -band -important for the analysis of graphene- shows a splitting for uniaxial strain. The splitting depends on the strength and direction of the applied strain and on the polarization of the incident and outgoing light. We expand the double-resonance Raman model in order to explain the strain direction dependence and the polarization dependence of the splitting. The analysis of this splitting gives new insight into the origin of the $2D$ -band. Our prediction of the strain direction and polarization dependence agrees well with recent experiments.

PACS numbers: 81.05.ue, 63.22.-m, 78.67.Wj

The discovery of graphene in 2004 has led to strong research activities in the last years[1]. Graphene has been shown to possess unique material properties. In graphene the quantum Hall effect was observed at room temperature [2, 3]. Because of the specific band structure near the Fermi level, the electrons behave like massless Dirac fermions and mimic relativistic particles with zero rest mass and with an effective 'speed of light' $c' \approx 10 \cdot 10^6$ m/s [2, 4]. The high electron mobility makes graphene a promising candidate to serve as building block for micro-electronics.

Detecting and characterizing graphene still is an experimentally difficult task, in particular, finding its crystallographic orientation. One method to specify graphene layers is Raman spectroscopy. This non-destructive method can be used at ambient conditions. It allows to distinguish between single-layer, bilayer, and multi-layers of graphene[5]. The quality of the graphene flakes can be estimated from Raman features[6]. Recently, uniaxially strained graphene has been investigated by Raman spectroscopy[7–9]. The strain softens the frequency of the optical phonon branches. Uniaxial strain also reduces the hexagonal symmetry of the system. This symmetry breaking leads to new effects, e.g. , the orientation of graphene can be determined from the polarization dependence of the split G-band[8, 9]. Because of the doping dependence of the G-band-frequency [10] and the higher shift rate of the $2D$ -mode the latter is more commonly used to quantify strain in graphene. The shift of the $2D$ -mode is currently under discussion and usually only a single value for all measurements is given.[8, 9, 11] However, recent experiments show that the shift of the $2D$ -mode in addition depends on the crystallographic orientation and the polarization of the incident and outgoing light during the Raman experiments.[12, 13] In addition, a splitting of the $2D$ -mode has been observed. To understand these new results a comprehensive theoretical description is needed to quantify the shift of the $2D$ -mode under strain and that takes into account the polarization and the crystallographic orientation.

Here we expand the established model of the double-resonance in graphene. We explicitly calculate the resonant Raman cross section which is used to identify the contributing phonons and to estimate a polarization dependence. The effect of small strain on the peak positions of the $2D$ mode of

graphene is investigated on the level of density-functional theory. The strain is applied along arbitrary directions. We are able to explain the splitting, the shift rates, the polarization effects and the crystallographic orientation dependence. The observed effects do not solely come from a movement of the Dirac cones or their deformation, but rather from an orientation dependent softening of the involved phonon TO branch. The large magnitude of the splitting can only be explained with phonons from the branches between the Γ and K -points that contribute to the double-resonant $2D$ -mode.

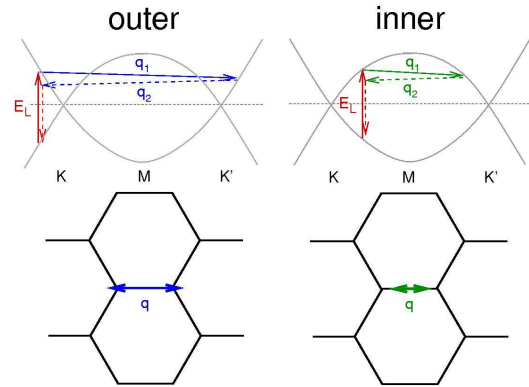


FIG. 1. Double-resonance mechanism (left: outer process, right: inner process) plotted into the band structure scheme of graphene along KMK' . Below is the mechanism plotted in the Brillouin zone.

In Fig. 1 we show the scheme of the double-resonance principle for the $2D$ -mode[14]. An electron-hole pair is created by an incoming photon with energy E_i . The electron or hole is scattered inelastically by a phonon with a wavevector $q_1 \neq 0$ into a real state. From there it scattered back inelastically by another phonon $q_2 = -q_1$, where it recombines with an energy $E = E_i - 2\hbar\omega(q_1)$. The difference to the $2D$ -mode is that for the D -mode, one inelastic scattering process is replaced by an elastic scattering at a defect. It is generally accepted, that the contributing phonons stem from the fully-symmetric TO-derived branch[15].

In the following we first use analytical expressions of the electronic and vibrational band structure to calculate Raman spectra for different scattering configurations. With these results we identify the dominant processes and motivate their

extraction from density functional theory (DFT) calculations under strain. The cross section $|K_{2f,10}|^2$ of a resonant Raman process can be calculated by[16]

$$K_{2f,10} = \sum_{a,b,c} \frac{M_{fc}M_{cb}M_{ba}M_{ai}}{(E_l - E_{ai} - i\hbar\gamma)(E_l - \hbar\omega - E_{bi} - i\hbar\gamma)(E_l - \hbar\omega - E_{ci} - i\hbar\gamma)} + \frac{M_{fc}M_{cb}M_{ba}M_{ai}}{(E_l - E_{ai} - i\hbar\gamma)(E_l - E_{bi} - i\hbar\gamma)(E_l - \hbar\omega - E_{ci} - i\hbar\gamma)} \quad (1)$$

This is the formula for the D -mode. The first term denotes incoming resonance, and the second outgoing resonance. E_{xy} is the energy difference between the electronic states x and y . E_l and $E_l - \hbar\omega$ are the energies of the incoming and outgoing photon, respectively. M_{xy} is the matrix element for the scattering over the intermediate states x and y , and γ is the broadening parameter of the electronic transition.

To investigate which processes contribute to the D -mode we evaluate Eq. (1). The sum is converted into an integral and the matrix elements are taken constant, although they may depend on the electronic wavevector. The electronic bands are from a tight-binding approach[17], where we use the values $\gamma_0 = 2.8$ eV and $\gamma_0' = 0$ eV. The TO phonon dispersion around the K -point is taken from the analytical expression derived from recent inelastic X-ray measurements [18].

In a first approximation we integrate along the line that connects two neighboring K -points [see Fig. 2(a)]. We have to take special care in this one-dimensional integration as it leads to erroneous results: in the one-dimensional integrations phonons with $q \approx K$ do not interfere destructively and give a major contribution[15]. Still, the one-dimensional integration gives a good idea for identifying the contributing processes. We find contributions from phonons from the $K - M$ and $\Gamma - K$ directions. The Raman matrix element $|K_{2f,10}|$ as a function of phonon frequency is plotted in Fig. 2(b). Here, a small broadening parameter of $\gamma = 0.005$ eV was used. The two peaks of the blue and green plot correspond to incoming and outgoing resonance.

In a second approximation we now look at the integration in two dimensions. The integration areas are highlighted as shaded areas in Fig. 2(a), where scattering into all neighboring K -valleys is considered. The integral is evaluated with the Monte-Carlo method provided in the Mathematica package (the method 'AdaptiveMonteCarlo' was used with at least 5×10^6 points)[19]. Now, the K -phonon contribution (not shown) is cancelled out due to destructive interference, in agreement with Ref. [15]. Comparing the result in Fig. 2(b) with the one-dimensional integration we find similar features. We thus can conclude that phonons from the $K - M$ direction and phonons from the $\Gamma - K$ direction do contribute to the D -mode in graphene. We will refer to them as outer processes (phonons from $K - M$, see Fig. 1) and inner processes (phonons from $\Gamma - K$). Using a larger value of $\gamma = 0.05$ eV, the distinct features merge and a single broad D -band arises [dotted curve in Fig. 2(b)].

In a perfect graphene flake the D -band does not depend on the polarization of the incident light. The polarization of the incoming laser affects the absorption in k -space. Electrons

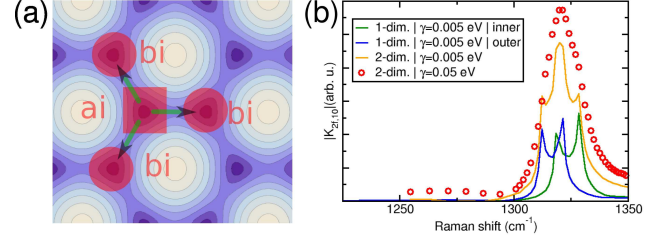


FIG. 2. (a) The two-dimensional integration area plotted in the electronic energy contours. The electron absorption happens near “ai” and the electron is scattered to regions near “bi”. (b) Raman matrix element $|K_{2f,10}|$ for several different parameter sets. Integration is either performed along lines connecting neighboring K -points (denoted by ‘1-dim.’) or two-dimensional within the highlighted area (‘2-dim.’). The similar features in both types of integration verifies that contributions from the inner processes are visible in the full calculation (two-dimensional integration) as well. At higher values of γ , single contributions are not distinguishable and a single D -peak is visible.

with a wavevector parallel to the polarization of a photon can not be excited during an absorption process. We include the effect of polarization by using the $|p \times k|^2$ -dependence of the absorption, where p denotes the polarization of the incident light and k denotes the wavevector of the excited electron[20]. This leads to areas in the Brillouin zone that give zero contribution to the Raman cross section. This is illustrated in Fig. 3(a) for “vertical” polarization indicated by the arrow \vec{p} . As expected and known from experiments, polarization of the incoming light has no influence on the D -band for unstrained graphene in Fig. 3(b). Now we simulate tensile strain, by compressing the band structure in strain-direction. This is indicated in Fig. 3(a) for strain in the zigzag direction. A strain of 9% was used. This is just a proof of concept, as we have not included the phonon softening, and used the unstrained phonon dispersion. The resulting Raman cross sections are shown in Fig. 3(b). The labels parallel and perpendicular are w.r.t. the strain direction. Depending on the polarization, the D -band has a different energy shift.

Using DFT calculations of the phonon dispersion and the electronic band structure we now make quantitative predictions on the peak positions of the 2D band for several scattering configurations. We have calculated the electronic bands and phonon dispersion of graphene under strain. These calculations were done with the linear-response DFT code QUANTUM-ESPRESSO[21, 22]. Uniaxial strain was applied via the two-dimensional strain tensor $\epsilon = ((\epsilon, 0), (0, -\epsilon\nu))$, where ν is the Poisson’s ratio. Strain in arbitrary directions has been applied through rotating the strain tensor[23]. The strain (tensile and compressive) is applied in several directions between the zigzag and armchair direction for strain values up to 3%. [22, 23] However, the largest differences are found between zigzag and armchair direction. With this data we can now perform a mapping of the expected $2D$ -band frequencies,

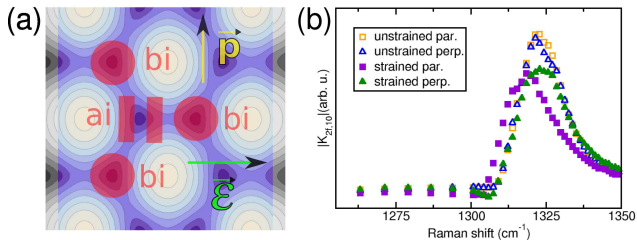


FIG. 3. (a) Modelling of strain by compressing the band structure. To account for the anisotropic absorption depending on the polarization, parts of the integration area have been omitted. (b) Raman matrix element $|K_{2f,10}|$ for strained and unstrained graphene with polarization parallel and perpendicular to the strain direction. Only when strain is applied, a polarization dependent shift is observed.

using the scattering processes shown in Fig. 1. The scattering of the electrons is considered to be elastic for identifying the contributing phonon's wavevector (this corresponds to horizontal arrows in Fig. 1).

Depending on which direction in reciprocal space the electron is scattered, different resonance conditions apply. This is a consequence of the symmetry-breaking induced by the strain.[24] In addition, as mentioned above, when the light is polarized, some areas in the reciprocal space do not have excited electrons that contribute to the $2D$ -band. With this argument the most dominant processes are those that are perpendicular to the polarization of the incoming light. Fig. 4 now show the obtained $2D$ frequencies for inner and outer processes (as depicted in Fig. 1), for strain in armchair (AC) and zigzag (ZZ) direction, and for two different laser energies (1.5 eV and 2.4 eV). The corresponding processes are illustrated in Fig. 5(a). The notation K_1 means along K_1 , the K -points are numbered clockwise, beginning with the top right as number 1. As can be seen, the splitting is larger for ZZ strain. Also the polarization dependent shift is larger for ZZ strain. Both, inner and outer processes lead to a polarization dependent splitting. However, the inner processes lead to a larger splitting. In Fig. 5(b) we show the phonon dispersion along two different paths in the reciprocal space. The TO branch between Γ and K shows a large splitting depending on the chosen path. The softening is stronger in the direction perpendicular to the strain direction. This can be understood looking at the displacement patterns of this mode: the displacement is parallel to the strain direction and the involved atomic bonds are weakened due to the strain. The same argument is responsible for the stronger softening of the G^- -mode at the zone-center[8, 9, 24]. Between K and M the displacement patterns of the TO branch are not parallel anymore and have lost their TO character and thus are not affected so strongly by the strain direction.

Biaxial strain was also applied to the system. In this case, the symmetry is conserved, there is no splitting. For the G -band we obtain a shift rate of $60 \text{ cm}^{-1}/\%$. This is in excellent agreement with the value of $63 \text{ cm}^{-1}/\%$ obtained in Ref. [25]

. For the $2D$ -band we find a shift rate of $135 \text{ cm}^{-1}/\%$ for both inner and outer processes.

With the above method of frequency mapping we cannot determine the details of intensity and lineshape of the D and $2D$ -bands. Simple arguments like looking at the electronic density of states do not take into account the phonon density of states. Sometimes it is argued that the outer processes only contribute to the $2D$ -mode because of the trigonal warping effect and a higher density of states[26, 27]: The trigonal warping effect becomes stronger for larger excitation energies, however for optical transition energies $< 2 \text{ eV}$ the equi-energy contours are still more or less round. In addition, the phonon dispersion of the TO-derived mode near the K -point was a long time believed to show a strong trigonal warping. This was recently resolved by Grüneis *et al.* performing inelastic x-ray experiments revealing almost-round equi-energy phonons of the TO-branch near the K -point[18] with almost no trigonal warping.

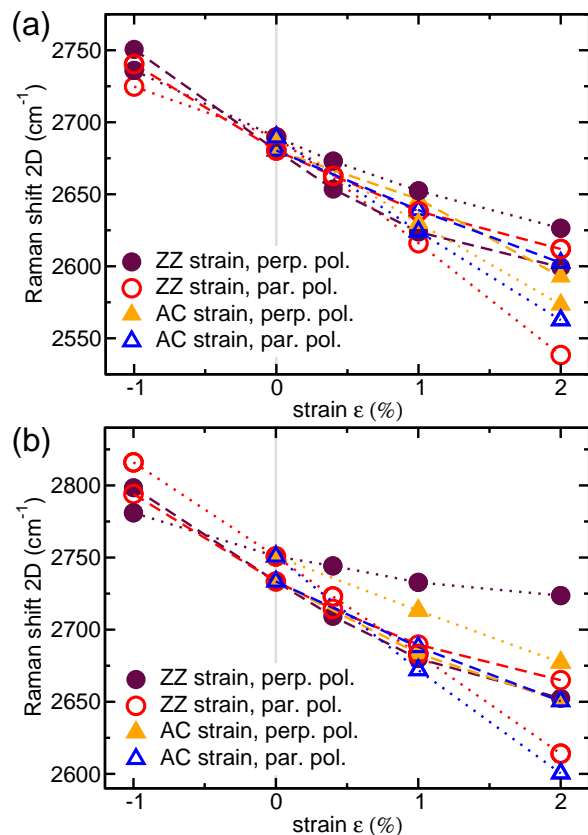


FIG. 4. Mapping of the Raman $2D$ contributions for inner and outer processes for the laser energies 1.5 eV (a) and 2.4 eV (b). Circles (triangles) correspond to strain in zigzag (armchair) directions. Open (closed) symbols denote parallel (perpendicular) polarization w.r.t. the strain direction. The data points are connected with lines that denote inner (dotted) and outer (dashed) processes.

In summary, we have presented an in-depth analysis of the evolution of the D and $2D$ -bands in uniaxially strained graphene. Depending on polarization and strain direction, different shifts of the Raman-active D and $2D$ -band are pre-

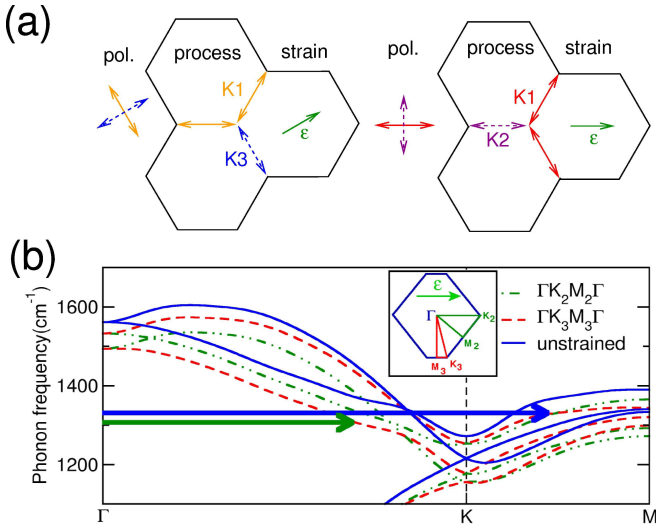


FIG. 5. (a) Dominant processes for perpendicular (solid lines) and parallel polarizations (dashed lines) for strain in ZZ and AC direction. (b) Optical phonon branch along Γ KM in graphene for unstrained (blue, solid line) and 2% strain in ZZ direction (green, dashed-dotted line and red, dashed line). The corresponding paths in the Brillouin zone are shown in the inset for an exaggerated strain of 30%. The dark grey (blue) arrow indicates the outer process for a laser energy of 2.4 eV, the grey (green) arrow indicates the inner process. Note that in absolute units of \AA^{-1} the three branches are slightly different due to strain (see inset). In the main figure we scaled the wavevector axis such that all K and M points are at the same position.

dicted. Strain in zigzag directions leads to a larger splitting than strain in armchair directions. Our predictions are in excellent agreement with experiments on strained graphene samples[12, 13]. As the strain-induced shift is used to determine strain in graphene our results are relevant for the interpretation of experimental data.

We would like to thank H. Yan, M. Huang, J. Hone, and T. Heinz from Columbia University and O. Frank, K. Papagelis, and C. Galiotis from University of Patras for sharing experimental results of Refs. 12, 13 prior to publication. JM and CT acknowledge support by the Cluster of Excellence 'Unifying Concepts in Catalysis' coordinated by the TU Berlin and funded by DFG.

* marcel@physik.tu-berlin.de

[1] K. S. Novoselov, A. K. Geim, S. V. Morozov, D. Jiang, Y. Zhang, S. V. Dubonos, I. V. Grigorieva, and A. A. Firsov, *Science* **306**, 666 (2004).
 [2] K. S. Novoselov, A. K. Geim, S. V. Morozov, D. Jiang, M. I. Katsnelson, I. V. Grigorieva, S. V. Dubonos, and A. A. Firsov, *Nature* **438**, 197 (2005).
 [3] Y. Zhang, Y.-W. Tan, H. L. Stormer, and P. Kim, *Nature* **438**, 201 (2005).
 [4] K. S. Novoselov, Z. Jiang, Y. Zhang, S. V. Morozov, H. L. Stormer, U. Zeitler, J. C. Maan, G. S. Boebinger, P. Kim, and

A. K. Geim, *Science* **315**, 1379 (2007).
 [5] A. C. Ferrari, J. C. Meyer, V. Scardaci, C. Casiraghi, M. Lazzeri, F. Mauri, S. Piscanec, D. Jiang, K. S. Novoselov, S. Roth, and A. K. Geim, *Phys. Rev. Lett.* **97**, 187401 (2006).
 [6] M. M. Lucchese, F. Stavale, E. H. M. Ferreira, C. Vilani, M. V. O. Moutinho, R. B. Capaz, C. A. Achete, and A. Jorio, *CARBON* **48**, 1592 (2010).
 [7] Z. H. Ni, T. Yu, Y. H. Lu, Y. Y. Wang, Y. P. Feng, and Z. X. Shen, *ACS Nano* **2**, 2301 (2008).
 [8] T. M. G. Mohiuddin, A. Lombardo, R. R. Nair, A. Bonetti, G. Savini, R. Jalil, N. Bonini, D. M. Basko, C. Galiotis, N. Marzari, K. S. Novoselov, A. K. Geim, and A. C. Ferrari, *Phys. Rev. B* **79**, 205433 (2009).
 [9] M. Huang, H. Yan, C. Chen, D. Song, T. F. Heinz, and J. Hone, *PNAS* **106**, 7304 (2009).
 [10] J. Yan, Y. Zhang, P. Kim, and A. Pinczuk, *Phys. Rev. Lett.* **98**, 166802 (2007).
 [11] G. Tsoukleri, J. Parthenios, K. Papagelis, R. Jalil, A. C. Ferrari, A. K. Geim, K. S. Novoselov, and C. Galiotis, *Small* **5**, 2397 (2009).
 [12] M. Huang, H. Yan, T. F. Heinz, and J. Hone, *Nano Lett.* **10**, 4074 (2010).
 [13] Private communication: O. Frank, University of Patras.
 [14] C. Thomsen and S. Reich, *Phys. Rev. Lett.* **85**, 5214 (2000).
 [15] J. Maultzsch, S. Reich, and C. Thomsen, *Phys. Rev. B* **70**, 155403 (2004).
 [16] M. Cardona, in *Light Scattering in Solids II*, Topics in Applied Physics, Vol. 50, edited by M. Cardona and G. Güntherodt (Springer, Berlin, 1982) p. 19.
 [17] P. R. Wallace, *Phys. Rev.* **71**, 622 (1947).
 [18] A. Grüneis, J. Serrano, A. Bosak, M. Lazzeri, S. L. Molodtsov, L. Wirtz, C. Attaccalite, M. Krisch, A. Rubio, F. Mauri, and T. Pichler, *Phys. Rev. B* **80**, 085423 (2009).
 [19] Wolfram Research, Inc., *Mathematica Edition: Version 6.0* (Wolfram Research, Inc., Champaign, Illinois, 2007).
 [20] A. Grüneis, R. Saito, G. G. Samsonidze, T. Kimura, M. A. Pimenta, A. Jorio, A. G. S. Filho, G. Dresselhaus, and M. S. Dresselhaus, *Phys. Rev. B* **67**, 165402 (2003).
 [21] P. Giannozzi, S. Baroni, N. Bonini, M. Calandra, R. Car, C. Cavazzoni, D. Ceresoli, G. L. Chiarotti, M. Cococcioni, I. Dabo, A. D. Corso, S. de Gironcoli, S. Fabris, G. Fratesi, R. Gebauer, U. Gerstmann, C. Gougoussis, A. Kokalj, M. Lazzeri, L. Martin-Samos, N. Marzari, F. Mauri, R. Mazzarello, S. Paolini, A. Pasquarello, L. Paulatto, C. Sbraccia, S. Scandolo, G. Sclauzero, A. P. Seitsonen, A. Smogunov, P. Umari, and R. M. Wentzcovitch, *J. Phys.: Condens. Matter* **21**, 395502 (2009).
 [22] Calculations were performed with the code QUANTUM-ESPRESSO[28]. We used a plane-wave basis set, RKKJ pseudopotentials[29] and the generalized gradient approximation in the Perdew, Burke and Ernzerhof parameterization for the exchange-correlation functional[30]. A Methfessel-Paxton broadening with a width of 0.02 Ry was used.[31] The valence electrons were expanded in a plane wave basis with an energy cutoff of 60 Ry. A $42 \times 42 \times 1$ sampling grid was used for the integration over the Brillouin zone. The dynamical matrices were calculated on a $12 \times 12 \times 1$ q -grid using the implemented linear-response theory. Force constants were obtained via a Fourier transformation and interpolated to obtain phonons at arbitrary points in the Brillouin zone.
 [23] For strain in arbitrary directions the strain tensor is rotated by $\epsilon' = \mathbf{R}^{-1}\epsilon\mathbf{R}$, where \mathbf{R} is the rotational matrix. After applying a finite amount of strain we relax the coordinates of the basis atoms until forces are below 0.001 Ry/a.u. and min-

- imize the total energy with respect to the Poisson's ratio ν . For small strain values we obtain a Poisson's ratio $\nu=0.164$, in excellent agreement with experimental tension measurements on pyrolytic graphite that yield a value of $\nu=0.163$. [32].
- [24] M. Mohr, K. Papagelis, J. Maultzsch, and C. Thomsen, Phys. Rev. B **80**, 205410 (2009).
- [25] C. Thomsen, S. Reich, and P. Ordejón, Phys. Rev. B **65**, 073403 (2002).
- [26] J. Kürti, V. Zolyomi, A. Grüneis, and H. Kuzmany, Phys. Rev. B **65**, 165433 (2002).
- [27] R. Narula and S. Reich, Phys. Rev. B **78**, 165422 (2008).
- [28] P. Giannozzi *et al.*, <http://www.quantum-espresso.org>.
- [29] A. M. Rappe, K. M. Rabe, E. Kaxiras, and J. D. Joannopoulos, Phys. Rev. B **41**, 1227 (1990).
- [30] J. P. Perdew, K. Burke, and M. Ernzerhof, Phys. Rev. Lett. **77**, 3865 (1996).
- [31] M. Methfessel and A. T. Paxton, Phys. Rev. B **40**, 3616 (1989).
- [32] O. L. Blakslee, D. G. Proctor, E. J. Seldin, G. B. Spence, and T. Weng, J. Appl. Phys. **41**, 3373 (1970).